Research Article | Vol. 26, No. 23 | 12 Nov 2018 | OPTICS EXPRESS 29895
Optics EXPRESS

Orbital angular momentum vector modes (de)multiplexer based on multimode micro-ring

SHIMAO LI,[1] ZHICHAO NONG,[1] XIONG WU,[1] WEN YU,[1] MINGBO HE,[1] CHARALAMBOS KLITIS,[2] YUNTAO ZHU,[1] SHENGQIAN GAO,[1] JIE LIU,[1] ZHAOHUI LI,[1] LIU LIU,[3,4] MARC SOREL,[2] SIYUAN YU,[1,5] AND XINLUN CAI[1,*]

[1]*State Key Laboratory of Optoelectronic Materials and Technologies and School of Physics and Engineering, Sun Yat-sen University, Guangzhou 510275, China*
[2]*School of Engineering, University of Glasgow, Rankine Building, Oakfield Avenue, Glasgow G12 8LT, UK*
[3]*South China Academy of Advanced Optoelectronics, South China Normal University, Guangzhou 510006, China*
[4]*realdream_liuliu@foxmail.com*
[5]*Department of Electrical and Electronic Engineering, University of Bristol, University Walk, Bristol, BS8 1TR, UK*
[*]*caixlun5@mail.sysu.edu.cn*

Abstract: Orbital angular momentum (OAM) multiplexing has emerged as an important method to increase the communication capacities in future optical information technologies. In this work, we demonstrate a silicon integrated OAM (de)multiplexer with a very simple structure. By simply tapping the evanescent wave of two different whispering gallery modes rotating inside a multimodal micro-ring resonator, four in-plane waveguide modes are converted to four free-space vector OAM beams with high mode purity. We further demonstrate chip-to-chip OAM multiplexing transmission using a pair of silicon devices, which shows low-level mode crosstalk and favorable link performance.

1. Introduction

Recently, spatial degree of freedom has attracted much attention for multiplexing information channel in addition to the time, wavelength and polarization dimensions [1]. Space based communication technique, also known as space-division multiplexing (SDM) [2,3], can be implemented in free space and optical fiber employing spatially orthogonal modes or spatial positions. The orbital angular momentum (OAM) beams containing helical phase fronts [4] are one set of orthogonal spatial modes. As a special case of mode-division multiplexing (MDM), OAM multiplexing has been demonstrated to be able to multiplicative increase transmission capacity in both free-space and optical fibre communications [5].

There have been several approached to the use of OAM mode basis for MDM communications in optical fibre. One approach aims to break the degeneracy within each mode group supported by ring core OAM fibres, therefore realising multiple-input multiple-output (MIMO) -free transmission [6]. Due to the limited achievable split in the mode effective refractive index between modes in the same group (typically in the 1~3e-4 range), this approach can only achieve short transmission distances. Another approach, which uses small scale modular MIMO to deal with mode coupling within each mode group, while relying on the large effective refractive index difference (typically in the 2~5e-3 range) between mode groups to achieve low inter-group coupling, has been shown to achieve longer transmission distances with low signal processing complexity [7]. Although such MDM schemes are not yet comparable to other schemes such as coupled core multi-core fibre, it

#331109 https://doi.org/10.1364/OE.26.029895
Journal © 2018 Received 7 May 2018; revised 26 Jul 2018; accepted 27 Sep 2018; published 31 Oct 2018

Optics EXPRESS

does support higher channel density per unit cross-sectional area, therefore worthy investigation for short to medium distance high capacity transmission.

One of the key challenges of realizing OAM-based telecommunications lies in creating high-performance OAM (de)multiplexers, which can transmit or receive multiple coaxially propagating OAM modes with low modal crosstalk and loss. To date, (de)multiplexing OAM modes have been routinely implemented by combinations of diffractive optical element and beam splitters [5,8]. The main issue associated with this approach is the scalability due to the inherent 1/N insertion loss of using cascaded beam splitters (N is the number of OAM modes). A more elegant solution is based on a device referred to as an OAM mode sorter [9–11], which can be used to (de)multiplex OAM modes with low crosstalk, and more importantly, does not experience the 1/N insertion loss that occurs during cascaded beam splitting. However, it still relies on large-scale (bulk) optical elements, which are vulnerable to even tiny changes in alignment. Photonic integration has been a major propellant for the widespread application of photonic technologies due to advantages in reliability, miniaturization, and scalability compared to bulk optics. Compact, robust, and efficient planar waveguide–based OAM (de)multiplexers are highly desirable, as they can be monolithically or hybridly integrated with other integrated components such as lasers, modulators and detectors, to form sophisticated photonic integrated circuits (PICs) with enhanced functionality. Previous implementations of on-chip OAM multiplexers relied on complicated phase-sensitive arrayed waveguide structures with many electrical contacts for phase calibration [12,13]. These devices typically had large footprints and complex control limitations. A compact and easy-to-use OAM mode (de)multiplexer is essential for realizing OAM-based telecommunications.

Previously, we demonstrated a silicon photonic OAM emitter based on grating assisted microring resonator [14]. The device has the advantages of ultra-compact size and simple operation. However, it is not a OAM multiplexer due to the fact that only two OAM modes can be excited by clock-wise or counter clock-wise whispering gallery modes (WGMs) at each resonance. Here, we report the first micro-ring-based demonstration of a compact on-chip OAM mode (de)multiplexing scheme based on the previous work. This (de)multiplexers have the advantages of compact footprint and simple operation compare to other SDM or MDM devices which need complicated phase control [15–17].

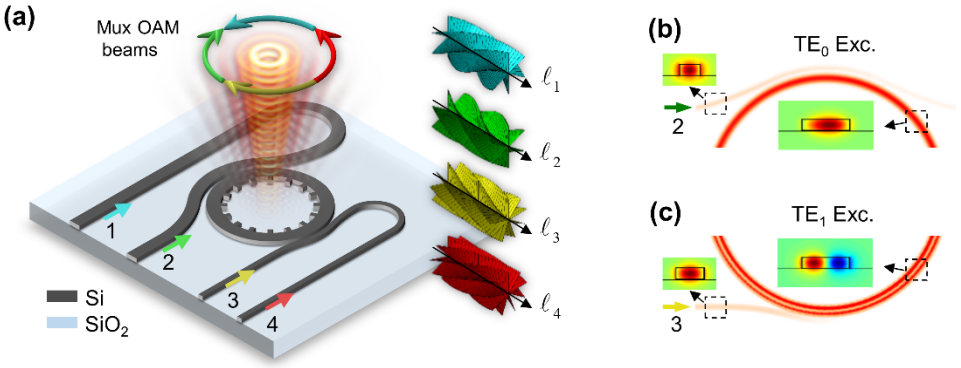

Fig. 1. (a) Schematic of an OAM MUX with a modified multimode micro-ring and two access waveguides (four ports) with different widths. (b) and (c) Selective coupling of fundamental mode in the access waveguides to TE_0 and TE_1 modes in the multimode micro-ring.

2. Design

The silicon photonic OAM mode multiplexer (MUX) comprises a multi-transverse micro-ring resonator with embedded angular grating structures [14] and two single-mode access waveguides with different widths, as shown in Fig. 1(a). The principle of operation of the

Optics EXPRESS

device is to couple TE0 modes from different access waveguides to rotating whispering gallery modes with different radial orders of the micro-ring resonator (see Figs. 1(b) and 1(c)). By matching the resonances of different WGMs, the angular grating elements within the resonator structure then couple different WGMs to multiple coaxially propagating OAM beams at the same wavelength. Conceptually, it is similar to our previous devices, but important change has been made. We use multi-transverse microring resonator to replace the single transverse microring resonator, making it possible to generate more than two OAM modes at the same wavelength, which will be detailed in the following sections.

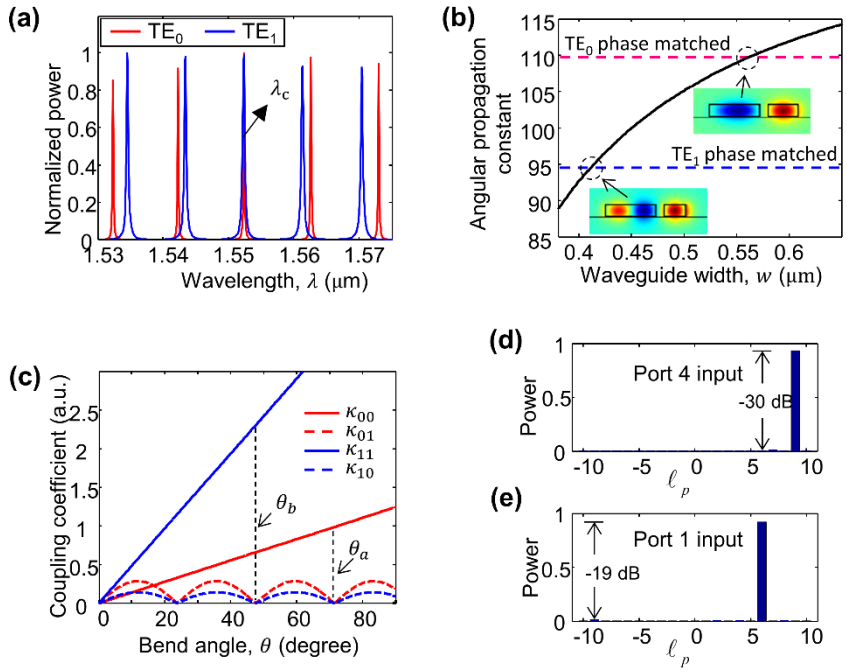

Fig. 2. (a) Simulated spectral responses of TE_0 and TE_1 WGMs in the micro-ring. (b) Calculated azimuthal propagation constant of the wrapped access waveguide as a function with waveguide width. Insets: one of the supermodes at positions where the azimuthal propagation constant of the access waveguide equal to the ones of the micro-ring waveguide. (c) Calculated coupling coefficients of the coupling region between the access waveguides (570-nm and 414-nm) and the multimode micro-ring as a function of the bend angle of the access waveguides. κ_{00}: 570-nm to TE_0. κ_{01}: 570-nm to TE_1. κ_{11}: 414-nm to TE_1. κ_{10}: 414-nm to TE_0. θ_a and θ_b are the positions where the desired mode is effectively coupled while the undesired mode is zero coupled for the 570-nm and 414-nm access waveguides, respectively. (d) and (e) Simulated mode purities of emitted beams with port 2 and 3 inputs, respectively.

The multimode micro-ring, formed from a bent waveguide of 976-nm-wide and 9.95-μm radius, is designed to support both TE_0 and TE_1 modes with azimuthal propagation constants (multiply propagation constants by the radius of the waveguide) of approximately 110 and approximately 95, respectively. The device parameters of the (de)multiplexer are carefully designed using finite difference time-domain (FDTD) method to make the resonances of TE_0 and TE_1 WGMs coincide at the target wavelength λ_c, as shown in Fig. 2(a).The two access waveguides are configured in a so-called "pulley-coupling" scheme [18–20], in which the waveguides wrap around the micro-ring resonator to form bent directional couplers (see Fig. 1(a)). The widths of the bent access waveguides are engineered to enable selective coupling to different WGMs in the micro-ring. A silicon photonic platform is attractive for this methodology because the propagation constants of waveguides can differ significantly due to

Optics EXPRESS

high index contrasts [21,22]. Figure 2(b) shows that for a bent access waveguide alongside a multimode micro-ring with a gap of 150 nm, a large range of azimuthal propagation constants of TE_0 modes ranging from 90 to 115 can be achieved by varying the waveguide width. By way of phase matching, the fundamental modes in the bent access waveguides can be evanescently coupled to a specific spatial mode in the adjacent multimode micro-ring waveguide, depending on the width of the single mode waveguide [20].

As shown in Fig. 2(b), when the access waveguide width is 570 nm or 414 nm, the azimuthal propagation constants of TE_0 modes in the access waveguides match the azimuthal propagation constants of the TE_0 WGM mode and the TE_1 WGM mode of the micro-ring, respectively, and therefore couple efficiently to the micro-ring. Figures 1(b) and 1(c) show such coupling of the TE_0 modes in different access waveguides to the TE_0 or TE_1 WGMs in the multimode micro-ring. According to [14], the WGMs are scattered by the angular grating embedded within the micro-ring, and the scattered beams are vector OAM beams with topological Pancharatnam charge:

$$\ell_p = p - q \tag{1}$$

where p is the number of optical periods of the WGM involved and q is the number of grating elements around the micro-ring. The input optical signals from the two access waveguides can excite two different mode orders at the wavelength λ_c, as the number of p is different for different transverse WGMs. Accounting for the fact that clockwise and anticlockwise modes that propagate in the micro-ring produce two states with equal but opposite mode orders [23], up to 4 vector OAM modes can be multiplexed. Rigorous theoretical derivation shows that the angular grating structure can be designed with low crosstalk between the different WGMs (see the supplementary materials in [14]).

To achieve good device performance, coupling through the micro-ring must be designed to minimize the power that is coupled to the undesired WGM mode as well as to minimize the insertion loss for the desired mode. This can be done by optimizing the coupling gap and the bending angle of the bent directional couplers. The desired and undesired coupling modes for TE_0 mode in the 570-nm-wide access waveguide, respectively, is TE_0 and TE_1 WGMs in micro-ring, and the reverse is true for TE_0 mode in the 414-nm-wide access waveguide. The coupling strengths between these modes, as functions of bending angle, can be computed based on coupled mode theory [20]. As depicted in Fig. 2(c), the coupling to the undesired modes is much weaker because of the phase mismatch with these modes. Furthermore, the crosstalk can be eliminated at certain bending angles (termed zero-crosstalk-points). Considering the requirements of both low crosstalk and low insertion loss, the bending angle must be set at one of the zero-crosstalk-points for the undesirable mode, and close to the "critical coupling [24]" for the desirable mode so that all of the input power enters the desirable mode. The bending angles of the 570-nm-wide and 414-nm-wide access waveguides are designed to be 71 degrees and 47 degrees, respectively, to achieve optimal crosstalk and loss performance (see simulation Figs. 2(d) and 2(e)). According to the principle of reciprocity, this device can also be used as a demultiplexer (DEMUX) that receives 4 specific OAM states and separates them into different waveguides according to their phase structures [23].

3. Fabrication and characterization

The micro-ring OAM (de)multiplexer was fabricated on a SOI wafer with 220-nm thick silicon core and 2-μm buried oxide layer. The micro-ring was defined with a radius of 9.95 μm, width of 976 nm and 104 grating elements of 80-nm width and 100-nm protruding length. One access waveguide was defined with a width of 570 nm and 50-degree arc, and another access waveguide was defined with a width of 414 nm and 28-degree arc. The separation gap between the micro-ring and both access waveguides is 150 nm. The device

Optics EXPRESS

was patterned using direct write electron beam lithography into a positive electron beam resist (ZEP520A). The silicon layer was then etched using inductively coupled plasma (ICP). The fabricated device was shown in Fig. 3(a).

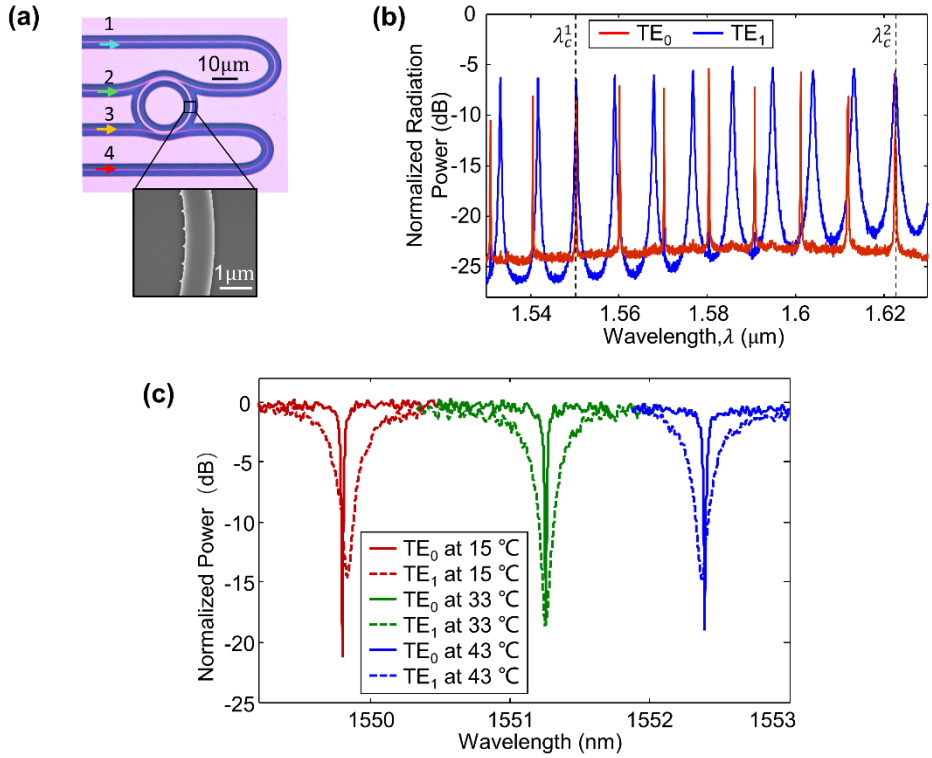

Fig. 3. (a) Microscopy image of the fabricated OAM (de)multiplexer. Inset: zoom- multiplexer SEM image showing the multimode waveguide of the micro-ring and the angular grating. (b) The radiation spectral responses measured by scanning input laser wavelength. (c) Transmission spectral response of the micro-ring TE_0 mode and TE_1 mode with different temperatures loaded in the substrate of the chip.

Figure 3(b) shows the emission spectral responses of the device with input optical signals from port 1 and port 3, one for TE_0 WGM and the other for TE_1 WGM. Each of the responses has a well-defined but different free spectrum range (FSR), which indicates successful selective WGM excitation in the micro-ring. The emission efficiencies (defined as the ratio of the emitted power over the optical power in the access waveguide) at various resonances are measured to be 9 to 30%. Some of the resonances were far from the critical coupling condition and then most of the optical power transmitted through the access waveguide, which lead to inefficient emission. The efficiencies can be improved by engineering optimized coupler for the ring and integrating a mirror below the angular grating to reduce down emitting loss [25]. It is observed that the resonances of TE_0 and TE_1 WGMs coincide at two wavelengths of λ_c^1 (1550 nm) and λ_c^2 (1622 nm), thus OAM multiplexing can be implemented at both wavelengths. It should be noted that the resonances of the micro-ring are very sensitive to the device parameters due to the high-index contrast of the SOI platform [26], and we use a thermal optical effect to address this issue. Due to the different temperature sensitivities of the micro-ring TE_0 and TE_1 modes, their relative resonant wavelengths can be tuned using the thermal-optic (TO) effect. The temperature sensitivity depends on modal confinement in silicon, i.e., the strong confined mode is more sensitive with temperature as

more fields localize into the silicon core, which has high TO coefficient. For a ring resonator, the temperature sensitivity of the resonant wavelength can be expressed as follows [27]:

$$\frac{d\lambda}{dT}=\left(\alpha\cdot n_e+\frac{dn_e}{dT}\right)\frac{\lambda}{n_g} \tag{2}$$

where λ is the resonant wavelength, T is the temperature, α is expansion coefficient, n_e is the effective index and n_g is the group index. For the TE_0 and TE_1 modes in a 9.95 μm radius micro-ring with 0.95 μm width, the temperature sensitivities near a wavelength of 1550-nm were calculated as approximately 78 pm/K and 76 pm/K, respectively. The calculation indicates that the resonant wavelength of the TE_0 mode shifts faster than that of the TE_1 mode with temperature, and therefore their resonant wavelengths can be relatively tuned to coincide when there is a small misalignment, as shown in Fig. 3(c). In future work, a resistive heater can be designed on top of the device in order to acquire local high temperature and realize large-range tuning of the resonances.

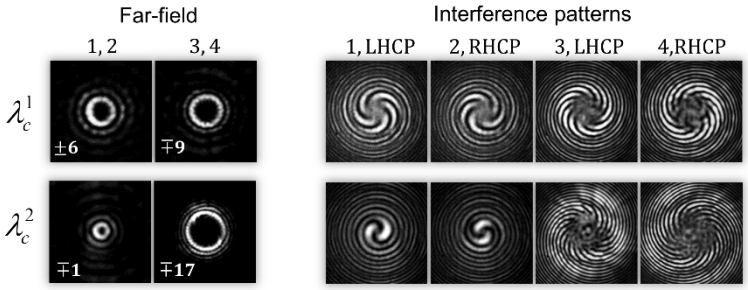

Fig. 4. Measured far-field intensity distributions of the radiated beams at coincident wavelengths of λ_c^1 (1550 nm) and λ_c^2 (1622 nm), and the interference patterns of its LHCP or RHCP with reference to the Gaussian beam.

Figure 4 shows the far-field intensity distributions of the emitted beams from different input ports at the two coincident resonances. Due to the phase singularity, all of the beams have are null on the axis. Following the procedure described in [14], the wave front structures of the generated beams were characterized using an interference scheme. The generated beam can be described as the superposition of a left-hand circularly polarized (LHCP) OAM beam with OAM value of ℓ_p-1 and a right-hand circularly polarized (RHCP) OAM beam with OAM value of ℓ_p+1. Therefore, when the beam is made to interfere with a RHCP (LHCP) Gaussian beam, a spiral intensity patterns with $|\ell_p+1|$ ($|\ell_p-1|$) arms is produced. The measured interference patterns (see Fig. 4) indicate that four vector OAM modes at λ_c^1 are generated independently from ports 1, 2, 3 and 4, and the topological charges are $\ell_p^1=-6$, $\ell_p^2=+6$, $\ell_p^3=+9$, and $\ell_p^4=-9$, respectively. Similarly, the generated OAM modes at λ_c^2 are $\ell_p^1=+1$, $\ell_p^2=-1$, $\ell_p^3=+17$, and $\ell_p^4=-17$, respectively. These results confirm that the device is capable of multiplexing four vector OAM modes at two wavelengths. It is noted that scalar OAM modes (with circular polarization) can also be generated from a ring resonator with optimized waveguide [28].

The mode purities of OAM modes play crucial roles in OAM multiplexing applications. In our devices, the deterioration of the mode purities may originate from undesired mode coupling in the bent directional coupler, and coupling between forward- and backward-travelling waves because of strong backscattering from roughness of the silicon waveguide. It

Optics EXPRESS

should be noted that there was barely backscattering from the grating of the device. According to the couple mode theory (see the supplementary materials of Ref [14].), the coupling between the *m*th mode and *n*th mode is insignificant when the following phase matching condition is not satisfied for all integer g :

$$v_m - v_n - gq = 0 \tag{3}$$

where v_m and v_n are the azimuthal propagation constants of the *m*th and *n*th modes, and q is the number of grating elements. For the device in our case, the angular propagation constants $|v_0|$ of the TE_0 WGM is 110, $|v_1|$ of the TE_1 WGM is 113, and q=104 , such that the four TE WGMs traveling in the ring are not satisfied Eq. (1) and then there is no significant coupling between them. An experimental setup based on a spatial light modulator (SLM), as shown in Fig. 5(a), was used to study the mode purities of the emitted OAM beams from the device [29]. After travelling through a quarter-wave plate and a polarizer, the RHCP or LHCP component of the beam was converted to a linearly polarized beam with an OAM value of $\ell_p - 1$ or $\ell_p + 1$, depending on the angle (− 45 or + 45-degree). The OAM value of the linearly polarized beam was then analyzed by changing the order of the holographic pattern on the SLM. If the order of the SLM hologram is the negative of the OAM value of the beam, then the resulting beam can be focused into a bright spot. The OAM power spectrum was then evaluated from the on-axis intensity of the images on an IR CCD array, which could be used to acquire mode purities of OAM modes (see Figs. 5(b) and 5(c)), and the mode purities of the OAM modes were measured to range from 87% to 97%.

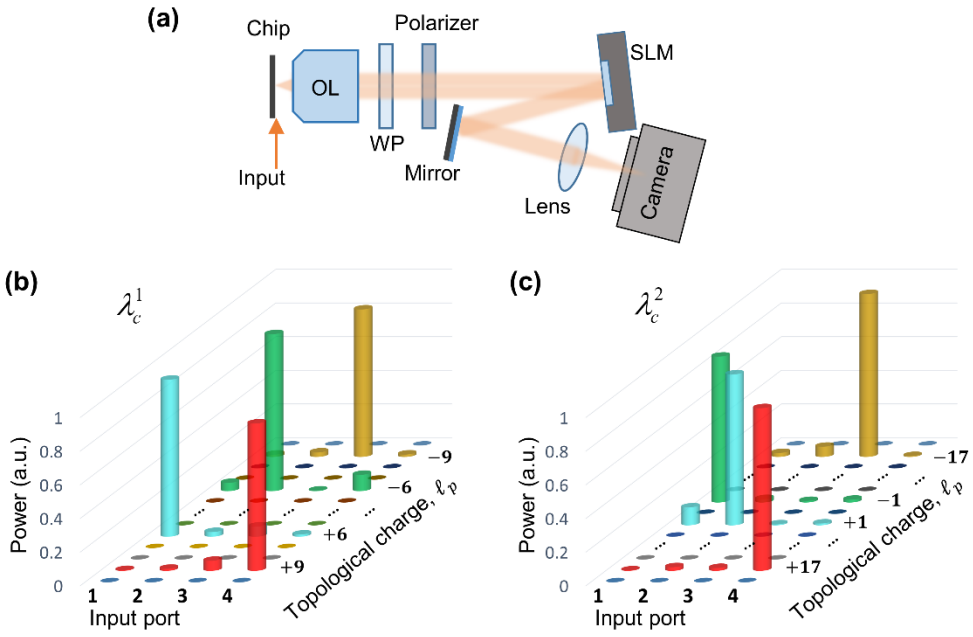

Fig. 5. (a) Experiment setup for measuring OAM purities. OL: objective lens. WP: quarter wave plate. (b) and (c) Mode purities of the emitted beams from the multiplexer versus the input ports at λ_c^1 and λ_c^2, respectively.

4. Chip-to-chip transmission

We present a proof-of-concept, chip-to-chip OAM multiplexing transmission experiment using two devices as the OAM MUX and DEMUX. Figure 6(a) shows the experimental setup for performance evaluation. The generated beams from the MUX are collected and collimated

Optics EXPRESS

through an aspherical lens (f=2.97 mm, NA = 0.6) and then directed to the DEMUX, where a second identical lens was used to focus the beam onto the modulated micro-ring. The DEMUX receives the beams and divides them into different output ports according their phase structure. In this axisymmetric configuration, when light is coupled into port 1 of the MUX, the generated ℓ_p^1 beam is directed to port 2 of the DEMUX; similarly, the MUX inputs at ports 2, 3, and 4 generate ℓ_p^2, ℓ_p^3 and ℓ_p^4 beams, and give outputs at the DEMUX ports 1, 4, and 3, respectively. The inset in Fig. 6(a) is a photo of the free-space optics and OAM devices, where the total length of the beam path is ~0.2-m. Using a Pitch Reducing Optical Fiber Array (PROFA) [30], optical signals can be coupled to all 4 input ports of MUX simultaneously. Output coupling is performed with a lensed fibre aligned to one output port at a time.

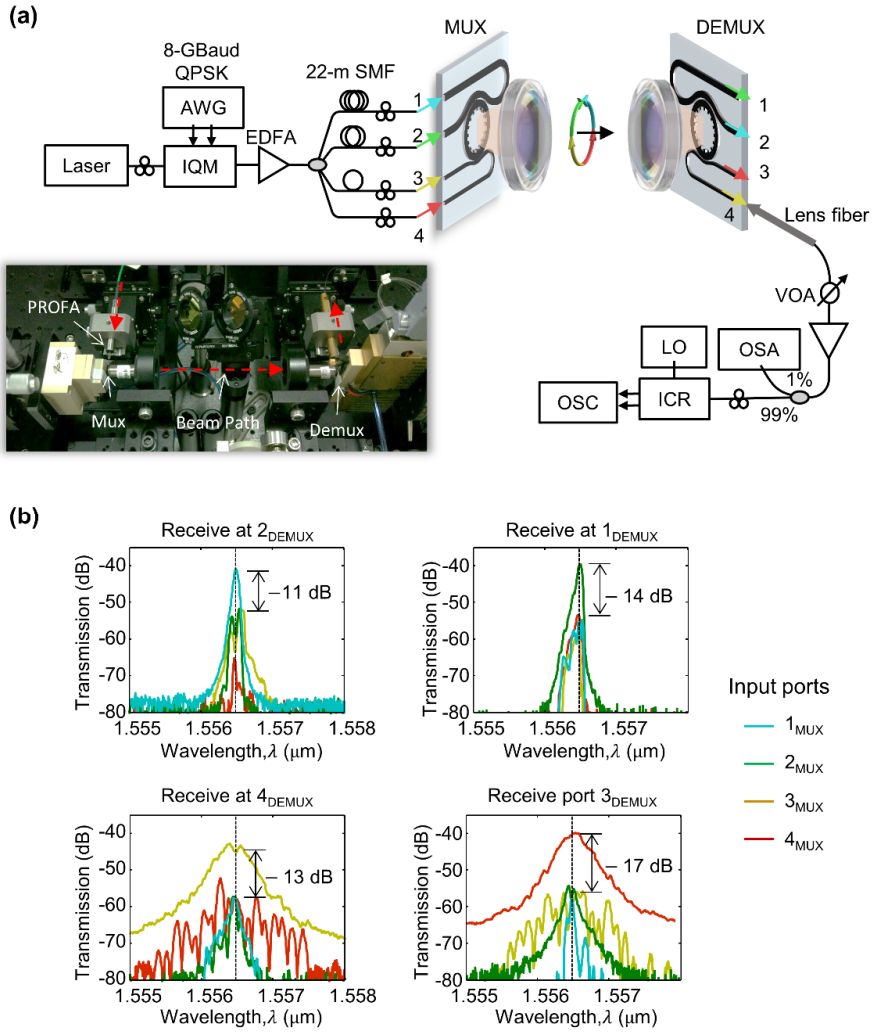

Fig. 6. (a) Experimental setup for performance evaluation of chip-to-chip transmission. PC: polarization controller. LF: lens fibre. VOA: variable optical attenuator. OSA: optical spectrum analyser. LO: local oscillator. Inset**:** photo of optics and two devices. (b) Optical transmission and crosstalk at the four output ports of DEMUX for optical injection on each of the four input ports of MUX.

Optics EXPRESS

Figure 6(b) plots the transmission responses at the DEMUX from each of the MUX ports near the coincidence wavelength of λ_c^1. At the coincidence wavelength, the crosstalk ranges from −13 to −17 dB. The insertion loss of our chip-to-chip experiment includes fibre-to-chip coupling loss (~5 dB), MUX -to-OAM coupling loss (~7 dB), lens transmitted and un-fully collected loss (~5 dB), OAM-to-DEMUX coupling loss (~18 dB) from setup misalignment and mode mismatch for the beam couple to the DEMUX ring, and chip-to-fibre coupling loss (5 dB). As the fill factor for the angular grating is small, the emission has considerable high-spatial-frequency component which cannot be fully collected by the lens with limited NA. The spatial-frequency loss through the two lens results the primary mode mismatch between the incident beam and the near-field mode of the DEMUX. Optimized experiment should use high-efficiency device with a bottom mirror to generate concentrated beam [25], and lens with high NA and large aperture to collect complete emission and suppress the diffraction of the propagating beam. The 3-dB bandwidth for channels of $\ell_p^{1,2}$ is 9 GHz, and for channels $\ell_p^{3,4}$ the bandwidth is 40 GHz. As the TE_0 is more confined in the waveguide width direction, the quality factor of the TE_0 mode is much higher than that of the TE_1 mode, hence the TE_0 has narrow bandwidth. In future work, the angular grating should be fabricated on top of the micro-ring [31], therefore all the WGMs will be effectively extracted to OAM modes.

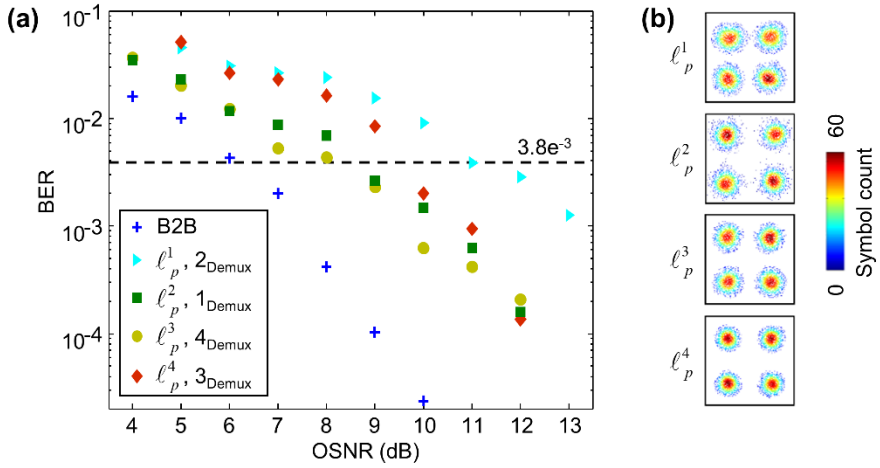

Fig. 7. (a) BER measurements for back-to-back (B2B) test case and OAM multiplexing operation for all four ports. (b) Corresponding constellation plots for the inspected signals.

We demonstrated the free-space OAM multiplexed transmission link where multiplexing 4-OAM states with injection at all MUX ports. Optical carrier from an external cavity laser (ECL) with wavelengths of λ_c^1 was modulated by an 8- GBaud QPSK signal generated from the arbitrary waveform generator (AWG) through an I/Q modulator (IQM). Then, the generated optical signal was amplified using erbium-doped fibre amplifiers (EDFA) and was split by optical couplers into four branches, which are decorrelated by single mode fibres (SMF) to generate four different signals. The four decorrelated QPSK signals were then launched into the MUX ports to generate the OAM multiplexed signals. After a certain distance transmission in free space, all four OAM modes were demultiplexed and converted to Gaussian beams using the DEMUX. In each branch after demultiplexing, the obtained Gaussian beam was coupled to SMF-pigtailed integrated coherent optical receivers (ICRs) for coherent optical detection. Then, the output electrical waveforms were recorded by a real-time oscilloscope (OSC) operated at 50-GSa/s and were digitally processed offline for bit-error-rate (BER) evaluation. The measured BER at different optical signal-to-noise ratios (OSNRs) of the transmission system is displayed in Fig. 7(a). The back-to-back (B2B) data

Optics EXPRESS

were taken without the MUX and DEMUX and instead a fibre attenuator provided an output power of −37 dBm (i.e., the highest DEMUX output). Compared to the B2B case, the OSNR penalties at BER of 3.8e-3 (the FEC limit corresponding to the hard-decision code 7% overhead) for OAM channels ℓ_p^1, ℓ_p^2, ℓ_p^3 and ℓ_p^4 are 4.8 dB, 2.4 dB, 1.8 dB and 3.3 dB, respectively, which verifies that the intra-channel crosstalk is the main mechanism of signal degradation. The larger penalty for state ℓ_p^1 is due to the significant increase of crosstalk with the modulated signal with a frequency spacing between the sidebands and the carrier (1550 nm), which can be observed in Fig. 6(b). Figure 6(b) presents the well-isolated constellation plots for OAM multiplexing transmission at OSNRs of 12 dB (ℓ_p^2, ℓ_p^3 and ℓ_p^4) and 13 dB (ℓ_p^1).

5. Discussion and conclusion

We have demonstrated CMOS-compatible integrated OAM (de)multiplexer on a SOI platform. While we have achieved up to four multiplexed OAM modes, the number of multiplexed modes can be increased by employing wider micro-ring waveguides with multiple access waveguides. As an example, when the width and the radius of the micro-ring waveguide is designed to be 1.1 μm and 19.144 μm, the device that can support six OAM modes. Moreover, the resonances of the device can also be designed to coincide at multiple wavelengths; therefore, our OAM multiplexing scheme is potentially compatible with WDM, which makes it very attractive for high capacity optical communications and optical interconnections.

The device benefits from its ultra-compact size, with a footprint that is two to three orders of magnitude smaller than previous demonstrations of integrated OAM multiplexing devices [12,13,32], and its extremely simple operation only requires a ring resonator and several access waveguides to couple the input optical signal. Different OAM modes can simply be addressed from different input ports. These advantages make it easy to integrate with other on-chip components to form sophisticated PICs with enhanced functionality, enabling large-scale integrated application opportunities for OAM beams.

Funding

National Natural Science Foundation of China (NSFC) (61490715, 11690031, 61622510, 61575224, 11690030); National Basic Research Program of China (2014CB340000).

References

1. P. J. Winzer, “Making spatial multiplexing a reality,” Nat. Photonics **8**(5), 345–348 (2014).
2. D. J. Richardson, J. M. Fini, and L. E. Nelson, “Space-division multiplexing in optical fiber,” Nat. Photonics **7**(5), 354–362 (2013).
3. N. Zhao, X. Li, G. Li, and J. M. Kahn, “Capacity limit of spatially multiplexed free-space communication,” Nat. Photonics **9**(12), 822–826 (2015).
4. L. Allen, M. W. Beijersbergen, R. J. C. Spreeuw, and J. P. Woerdman, “Orbital angular momentum of light and the transformation of Laguerre-Gaussian laser modes,” Phys. Rev. A **45**(11), 8185–8189 (1992).
5. A. E. Willner, H. Huang, Y. Yan, Y. Ren, N. Ahmed, G. Xie, C. Bao, L. Li, Y. Cao, Z. Zhao, J. Wang, M. P. J. Lavery, M. Tur, S. Ramachandran, A. F. Molisch, N. Ashrafi, and S. Ashrafi, “Optical communications using orbital angular momentum beams,” Adv. Opt. Photonics **7**(1), 66–106 (2015).
6. N. Bozinovic, Y. Yue, Y. Ren, M. Tur, P. Kristensen, H. Huang, A. E. Willner, and S. Ramachandran, “Terabit-scale orbital angular momentum mode division multiplexing in fibers,” Science **340**(6140), 1545–1548 (2013).
7. G. Zhu, Z. Hu, X. Wu, C. Du, W. Luo, Y. Chen, X. Cai, J. Liu, J. Zhu, and S. Yu, “Scalable mode division multiplexed transmission over a 10-km ring-core fiber using high-order orbital angular momentum modes,” Opt. Express **26**(2), 594–604 (2018).
8. J. Wang, J. Yang, I. M. Fazal, N. Ahmed, Y. Yan, H. Huang, Y. Ren, Y. Yue, S. Dolinar, M. Tur, and A. E. Willner, “Terabit free-space data transmission employing orbital angular momentum multiplexing,” Nat. Photonics **6**(7), 488–496 (2012).

Optics EXPRESS

9. M. P. J. Lavery, D. J. Robertson, G. C. G. Berkhout, G. D. Love, M. J. Padgett, and J. Courtial, "Refractive elements for the measurement of the orbital angular momentum of a single photon," Opt. Express **20**(3), 2110–2115 (2012).
10. H. Huang, G. Milione, M. P. J. Lavery, G. Xie, Y. Ren, Y. Cao, N. Ahmed, T. An Nguyen, D. A. Nolan, M. J. Li, M. Tur, R. R. Alfano, and A. E. Willner, "Mode division multiplexing using an orbital angular momentum mode sorter and MIMO-DSP over a graded-index few-mode optical fibre," Sci. Rep. **5**, 14931 (2015).
11. S. Lightman, G. Hurvitz, R. Gvishi, and A. Arie, "Miniature wide-spectrum mode sorter for vortex beams produced by 3D laser printing," Optica **4**(6), 605–610 (2017).
12. C. R. Doerr and L. L. Buhl, "Circular grating coupler for creating focused azimuthally and radially polarized beams," Opt. Lett. **36**(7), 1209–1211 (2011).
13. T. Su, R. P. Scott, S. S. Djordjevic, N. K. Fontaine, D. J. Geisler, X. Cai, and S. J. B. Yoo, "Demonstration of free space coherent optical communication using integrated silicon photonic orbital angular momentum devices," Opt. Express **20**(9), 9396–9402 (2012).
14. X. Cai, J. Wang, M. J. Strain, B. Johnson-Morris, J. Zhu, M. Sorel, J. L. O'Brien, M. G. Thompson, and S. Yu, "Integrated Compact Optical Vortex Beam Emitters," Science **338**(6105), 363–366 (2012).
15. C. R. Doerr and T. F. Taunay, "Silicon Photonics Core-, Wavelength-, and Polarization-Diversity Receiver," IEEE Photonics Technol. Lett. **23**(9), 597–599 (2011).
16. A. M. J. Koonen, H. Chen, H. P. A. van den Boom, and O. Raz, "Silicon Photonic Integrated Mode Multiplexer and Demultiplexer," IEEE Photonics Technol. Lett. **24**(21), 1961–1964 (2012).
17. Y. Ding, H. Ou, J. Xu, and C. Peucheret, "Silicon Photonic Integrated Circuit Mode Multiplexer," IEEE Photonics Technol. Lett. **25**(7), 648–651 (2013).
18. M. K. Chin and S. T. Ho, "Design and Modeling of Waveguide-Coupled Single-Mode Microring Resonators," J. Lightwave Technol. **16**(8), 1433–1446 (1998).
19. J. Hu, N. Carlie, N. N. Feng, L. Petit, A. Agarwal, K. Richardson, and L. Kimerling, "Planar waveguide-coupled, high-index-contrast, high-Q resonators in chalcogenide glass for sensing," Opt. Lett. **33**(21), 2500–2502 (2008).
20. E. Shah Hosseini, S. Yegnanarayanan, A. H. Atabaki, M. Soltani, and A. Adibi, "Systematic design and fabrication of high-Q single-mode pulley-coupled planar silicon nitride microdisk resonators at visible wavelengths," Opt. Express **18**(3), 2127–2136 (2010).
21. M. K. Chin, C. W. Lee, S. Y. Lee, and S. Darmawan, "High-index-contrast waveguides and devices," Appl. Opt. **44**(15), 3077–3086 (2005).
22. L. W. Luo, N. Ophir, C. P. Chen, L. H. Gabrielli, C. B. Poitras, K. Bergmen, and M. Lipson, "WDM-compatible mode-division multiplexing on a silicon chip," Nat. Commun. **5**(1), 3069 (2014).
23. K. Cicek, Z. Hu, J. Zhu, L. Meriggi, S. Li, Z. Nong, S. Gao, N. Zhang, X. Wang, X. Cai, M. Sorel, and S. Yu, "Integrated optical vortex beam receivers," Opt. Express **24**(25), 28529–28539 (2016).
24. A. Yariv, "Critical coupling and its control in optical waveguide-ring resonator systems," IEEE Photonics Technol. Lett. **14**(4), 483–485 (2002).
25. S. Li, Y. Ding, X. Guan, H. Tan, Z. Nong, L. Wang, L. Liu, L. Zhou, C. Yang, K. Yvind, L. K. Oxenløwe, S. Yu, and X. Cai, "Compact high-efficiency vortex beam emitter based on a silicon photonics micro-ring," Opt. Lett. **43**(6), 1319–1322 (2018).
26. W. Bogaerts, P. D. Heyn, T. V. Vaerenbergh, K. D. Vos, S. K. Selvaraja, T. Claes, P. Dumon, P. Bienstman, D. V. Thourhout, and R. Baets, "Silicon microring resonators," Laser Photonics Rev. **6**(1), 47–73 (2012).
27. J. Teng, P. Dumon, W. Bogaerts, H. Zhang, X. Jian, X. Han, M. Zhao, G. Morthier, and R. Baets, "Athermal Silicon-on-insulator ring resonators by overlaying a polymer cladding on narrowed waveguides," Opt. Express **17**(17), 14627–14633 (2009).
28. Z. Shao, J. Zhu, Y. Chen, Y. Zhang, and S. Yu, "Spin-orbit interaction of light induced by transverse spin angular momentum engineering," Nat. Commun. **9**(1), 926 (2018).
29. Q. Xiao, C. Klitis, S. Li, Y. Chen, X. Cai, M. Sorel, and S. Yu, "Generation of photonic orbital angular momentum superposition states using vortex beam emitters with superimposed gratings," Opt. Express **24**(4), 3168–3176 (2016).
30. F. E. Doany, B. G. Lee, S. Assefa, W. M. J. Green, M. Yang, C. L. Schow, C. V. Jahnes, S. Zhang, J. Singer, V. I. Kopp, J. A. Kash, and Y. A. Vlasov, "Multichannel high-bandwidth coupling of ultradense silicon photonic waveguide array to standard-pitch fiber array," J. Lightwave Technol. **29**(4), 475–482 (2011).
31. Z. Shao, J. Zhu, Y. Zhang, Y. Chen, and S. Yu, "On-chip switchable radially and azimuthally polarized vortex beam generation," Opt. Lett. **43**(6), 1263–1266 (2018).
32. B. Guan, R. P. Scott, C. Qin, N. K. Fontaine, T. Su, C. Ferrari, M. Cappuzzo, F. Klemens, B. Keller, M. Earnshaw, and S. J. B. Yoo, "Free-space coherent optical communication with orbital angular, momentum multiplexing/demultiplexing using a hybrid 3D photonic integrated circuit," Opt. Express **22**(1), 145–156 (2014).